International Journal of Nanomedicine

Dovepress
Taylor & Francis Group

Open Access Full Text Article

ORIGINAL RESEARCH

Astragalus Polysaccharide Nanoparticles Alleviate Sepsis-Induced Myocardial Injury by Targeting the HSP90AA1/NLRP3 Signaling Pathway

Xiong Yue[1,2], Meimei Hu[2], Cunmin Zhou[2], Bangyun Tan[2], Xiaoying Xu[1,2]

[1]The First Clinical Medical College, Lanzhou University, Lanzhou, Gansu, People's Republic of China; [2]Department of Clinical Laboratory, The First Hospital of Lanzhou University, Lanzhou, Gansu, People's Republic of China

Correspondence: Xiaoying Xu, Department of Clinical Laboratory, The First Hospital of Lanzhou University, 1 West Dong Gang Road, Lanzhou, Gansu, People's Republic of China, Tel +86-0931-8356353, Email xiaoying.1123@163.com

Purpose: This study aimed to investigate the mechanisms by which Astragalus polysaccharide nanoparticles (APS-CS/TPP) protect against septic myocardial injury, addressing the limited understanding of how APS-CS/TPP specific signaling pathways in this condition.

Materials and Methods: Potential targets and pathways of Astragalus polysaccharide (APS) were initially predicted using network pharmacology, molecular docking, and microscale thermophoresis. APS-CS/TPP were prepared using an ion gel method with a chitosan derivative and characterized for formation, size, and surface charge. A murine model of septic myocardial injury was established by cecal ligation and puncture (CLP), and therapeutic outcomes were assessed via echocardiography, ELISA, histology, and Western blot. In vitro, H9c2 cells were stimulated with LPS and treated with APS-CS/TPP, with or without the HSP90AA1 inhibitor TAS-116, followed by evaluation of inflammatory markers and protein expression.

Results: APS showed high binding affinity to HSP90AA1. APS-CS/TPP improved survival and attenuated myocardial damage in septic mice. In vitro, they reduced levels of IL-1β, IL-6, and TNF-α, and downregulated HSP90AA1, NLRP3, caspase-1, and IL-1β. These effects were suppressed by TAS-116.

Conclusion: APS-CS/TPP protect against septic myocardial injury by inhibiting the HSP90AA1/NLRP3 signaling pathway.

Keywords: nanoparticles, HSP90AA1, NLRP3, cardioprotection, astragalus polysaccharide

Introduction

Sepsis, characterized by a dysregulated host response to infection leading to organ dysfunction, remains a major cause of global morbidity and mortality.[1,2] The heart is particularly vulnerable in sepsis,[3] and effective therapies to prevent or treat septic myocardial injury are limited, with current management relying mainly on supportive care and antibiotics.[4]

The NOD like receptor protein 3 (NLRP3) inflammasome plays a central role in the pathogenesis of septic myocardial injury,[5,6] promoting inflammation, cardiomyocyte apoptosis, and cardiac dysfunction.[7] Although inhibition of the NLRP3 pathway represents a promising therapeutic strategy, its upstream regulation in sepsis is not fully understood.

Heat Shock Protein 90 Alpha Family Class A Member 1 (Hsp90AA1) maintained the stability of NLRP3 by guarding it.[8] It has been reported that the overexpression of Hsp90AA1 activated innate immunity via NLRP3 signaling pathways in yellow catfish.[9] In response to the priming signal, the removal HSP90AA1 led to the NLRP3 inflammasome triggering the cleavage of pro-caspase-1 into active caspase-1, which then promoted the secretion of inflammatory cytokines, including IL-1β, TNF-α, and IL-6.[10] A recent study further demonstrated that the HSP90AA1 inhibitor TAS-116 effectively degraded NLRP3 and attenuated inflammasome activation in rats with ulcerative colitis.[11] In addition to maintaining stability, HSP90AA1 was also implicated in DNA repair, immune response, neurodegenerative diseases, and heat stress response.[12] HSP90AA1 has been shown to stabilize NLRP3 and facilitate inflammasome activation in other inflammatory conditions, yet its role in septic cardiomyopathy remains unclear.

https://doi.org/10.2147/IJN.S580840
Received: 27 November 2025
Accepted: 17 February 2026
Published: 25 February 2026

Astragalus polysaccharide (APS) exhibits anti-inflammatory and cardioprotective properties and has been reported to inhibit NLRP3 signaling.[13,14] However, its clinical translation is limited by poor cellular uptake due to its macromolecular structure.[15] To address this, we developed Astragalus polysaccharide nanoparticles (APS-CS/TPP) using a chitosan-based delivery system. Previous studies demonstrated that, at an equivalent dose, these nanoparticles outperform plain APS by markedly lowering the bacterial load in peripheral blood, attenuating inflammatory markers, and reducing levels of myocardial injury-specific indicators in sepsis models, thereby conferring protection against septic myocardial injury.[16] Nevertheless, the precise mechanism underlying the cardioprotective effect of APS-CS/TPP in sepsis remains unclear.

Therefore, this study aimed to investigate whether APS-CS/TPP attenuate septic myocardial injury by targeting HSP90AA1 and inhibiting the NLRP3 inflammasome pathway. Using integrated network pharmacology, molecular docking, and experimental validation in vivo and in vitro, we hypothesized that APS-CS/TPP exert cardioprotective effects by suppressing the HSP90AA1/NLRP3 signaling axis. This study revealed the protective effect of APS-CS/TPP, provided a brand-new drug candidate strategy for the treatment of septic myocardial injury.

Materials and Methods

Network Pharmacology Research

The HERB database (http://herb.ac.cn/) was utilized to screen for the related chemical components of APS. Subsequently, their SMILES (Simplified Molecular Input-Line Entry System) representations were acquired via the PubChem database (https://pubchem.ncbi.nlm.nih.gov/) and uploaded to the Swiss Target Prediction database (http://www.swisstargetprediction.ch/) to find the bioactive components. The species chosen was "Homo sapiens" and the search results were fifiltered and deduplicated. "Septic myocardial injury" was used as a keyword to screen disease targets through the GeneCards database (https://www.genecards.org), the OMIM database (https://omim.org/), and the DrugBank database (https://go.drugbank.com/). Subsequently, with the aid of a Venn diagram (http://bioinformatics.psb.ugent.be/Webtools/Venn/), the overlapping targets were identified as the potential targets of APS against septic myocardial injury. The pathway enrichment analysis was performed using the DAVID database (https://david.ncifcrf.gov/) to explore the signal pathways with $P < 0.05$ as the screening condition. These KEGG pathways were visualized through the microletter online platform (http://www.bioinformatics.com.cn/). The component-target-pathway-disease network was visualized using Cytoscape software (version 3.7.2). The STRING 11.0 database (https://string-db.org/) was utilized to construct the Protein-Protein Interaction (PPI) network information which was set as Homo sapiens and high confidence of 0.700, and the key targets were screened by Cytoscape software (version 3.7.2). Subsequently, the hub genes were identified using six topological analysis methods (MCC, MNC, Degree, Stress, EPC, Bottleneck) commonly provided by the Cytohubba plugin of Cytoscape software (version 3.7.2) to evaluate and select hub targets.

Molecular Docking Analysis

Molecular docking technology was performed to predict the binding affinity of the hub target protein to active compounds. Generally, the crystal structures of hub targets were downloaded from the Protein Data Bank (http://www.rcsb.org/pdb). The MOL2 format of APS as the ligand was obtained from the TCMSP database. The processed ligand was then molecularly docked with the target protein using Autodock Vina 1.5.7 software to evaluate the interaction between key bioactive ingredients and the target proteins. Compounds with lower binding energy values were selected. Finally, PyMOL 2.3.4 software was utilized to analyze and visualize the docking results.

Microscale Thermophoresis Analysis

The binding of HSP90AA1 and APS was detected by Microscale thermophoresis (MST) with Monolith NTTM Protein labeling kits according to the instruction. Firstly, the NT-647-NHS-labeled HSP90AA1 was performed. Briefly, 100 μL HSP90AA1 protein was transfered to column A. Then mixed with 93μL labelling buffer and 7 μL dye into supernatant and placed it on ice Incubating in the dark for 30 minutes. Transfer 300 μL of the purified TMV protein solution to NHS-647 dye and mix very well by pipetting up and down several times. Subsequently, the labeled HSP90AA1 protein was

collected through filling in column B. A total of 16 gradient dilutions of APS were prepared beginning at a concentration of 100 μM. 10 μL NT-647-NHS-labeled HSP90AA1 was mixed well by pipetting up and down several times with different concentrations of 16 series of APS. Then all the samples were transfered to standard glass capillaries and measured using the MO. Control software to obtain the fitted curve and Kd value.

Components of APS

The ingredients of APS were roughly characterized by high-performance liquid chromatography (HPLC). 5 mg of APS samples was precisely weighed separately in one screw-cap tube. Then, 2 mL of trifluoroacetic acid was precisely added to the tube, sealed and hydrolyzed in an oven at 100°C for 4 hours. 2 mL of methanol was used to compensate for weight loss. Subsequently, dissolved the residue in 1 mL of ultrapure water to obtain the astragalus polysaccharide hydrolysate. After that, 200 μL of 1-phenyl-3-methyl-5-pyrazolone (PMP) and 200 μL 0.3 mol/L sodium hydroxide solution were mixed and incubated at 70°C for 30 minutes. After sample solutions were cooled to room temperature, the extracted solutions were extracted three times with an equal volume of chloroform, and the supernatant was then filtered by 0.22 μm millipore filter.

Preparation and Characteration of APS-CS/TPP

APS-CS/TPP were prepared using the ionic gelation technique as mentioned in our previous method.[16] Typically, a 1mg/mL TPP solution was added dropwise to a 2mg/mL chitosan acetic acid solution under magnetic stirring for 10 minutes. Subsequently, 10mg of APS was introduced and the mixture was stirred magnetically overnight at room temperature. Following a 60-minute centrifugation at 16,000 r/min, the precipitate was washed three times with 75% ethanol and then with distilled water. Finally, it was transformed into powder using a vacuum freeze dryer. To confirm the successful preparation of APS-CS/TPP, fourier Transform Infrared spectrometer (SPECTRUM 1000, Pontypool, UK) was employed to detect the absorption peaks of both APS and the APS-CS/TPP. At the same time, the prepared APS-CS/TPP was utilized to measure the nanoparticle size and ZETA potential using a particle size and ZETA potential analyzer (ZETASIZER Pro; Malvern, UK).

Animal Feeding and Treatment

C57BL/6 male mice (8–10 weeks old, n=82) were obtained from the Experimental Animal Center of Lanzhou University and fed a standard laboratory diet in the SPF Grade Trial Animal Center of Lanzhou University. Mice were randomly assigned to three groups: sham (n = 22), model control (CLP group, n=30), and Astragalus polysaccharides nanoparticles (CLP+APS-CS/TPP group, n=30). The CLP+APS-CS/TPP group received daily gavage administration of 200mg/kg APS-CS/TPP for three consecutive days prior to the establishment of the CLP model, as described in our previous method.[16] Equal volumes of saline were orally administered to both the sham and CLP groups. After an 8-hour fast, the mice underwent CLP surgery. A 1–2 cm midline incision was made to expose the cecum, which was then tightly ligated 1.5 cm from the tip and punctured with double holes17. Sham mice underwent the same procedure, except for the ligation and puncture. Administer APS-CS/TPP (at a dose of 200 mg/kg) by gavage every six hours after CLP surgery, lasting for 48 hours. Mice were humanely euthanized after 24 hours, and tissue samples were collected for analysis.

Cell Line and Infection

The H9c2 cardiomyocyte cell line (RRID:CVXL_0286, Wuhan Savier Biotechnology Co., Ltd., China) was cultured in DMEM supplemented with 10% fetal bovine serum (ExCell Bio, Australia), at 37 °C in 5% CO2. Upon reaching 80% confluence, the cells were divided into five groups: Control group (control), model control group (LPS+PBS), APS-CS /TPP group (LPS+APS-CS/TPP), model + HSP90AA1 inhibitor group (LPS+TAS-116), Model + HSP90AA1 inhibitor + APS-CS/TPP group (LPS+TAS-116+APS-CS/TPP). The LPS+PBS group was treated with 10μg/mL LPS for 24 hours, followed by the addition of 10 μL PBS and incubation for another 24 hours. The LPS+APS-CS/TPP group was treated with 10μg/mL LPS for 24 hours, followed by incubation with 50μg/mL APS-CS/TPP for 24 hours. The LPS+TAS-116 group was treated with 10μg/mL LPS for 24 hours, followed by incubation with 0.2 mg/mL TAS-116 for 24 hours. The LPS+TAS-116+APS-CS/TPP group was treated with 10 μg/mL LPS for 24 hours, followed by incubation with 0.2 mg/

mL TAS-116 for 4 hours, and then incubation with 50 μg/mL APS-CS/TPP for 20 hours. The Control group was incubated with PBS for 48 hours.

Transthoracic Echocardiography

Eight hours after CLP surgery, echocardiographic assessment was performed using a transesophageal echocardiography device specifically designed for animals (VisualSonics, 3080 Yonge St, Canada) to evaluate acute changes in cardiac function. The mice were anesthetized with 3% isoflurane and subsequently immobilized for molding. Ultrasound imaging was conducted using a 57-MHz probe. Subsequently, a series of M-mode images were obtained at the level of the left ventricular end-diastolic dimension (LVDd), end-systolic dimension (LVDs), stroke volume (SV), and cardiac output (CO). The Teichholz formula was used to estimate the left ventricular fractional shortening (LVFS), and the ejection fraction (LVEF) was measured using Vevo LAB 3.0.0. All measurements were based on three consecutive cardiac cycles.

HE Staining

Forty-eight hours after CLP, hematoxylin and eosin (H&E) staining was performed to observe more comprehensive pathological morphological changes in the myocardial structure of mice. The mouse myocardial tissues were fixed with 4% paraformaldehyde and subsequently embedded in paraffin, cut into sections 4 μm thick. The sections were then dewaxed, hydrated, and stained using H&E (Baso, Zhuhai Beso Biotechnology Co., China) following the manufacturer's protocol. An optical microscope (Olympus CX22, Japan) was used to observe the histopathological changes.

Enzyme-Linked Immunosorbent Assay

Forty-eight hours after CLP surgery, an ELISA kit from Jiangsu Enzyme Biotechnology Industrial Co., Ltd. was used to detect acute-phase changes in myocardial injury markers in mice, including cardiac troponin T (cTnT), lactate dehydrogenase (LDH), and creatine kinase-MB (CK-MB). The levels of cTnT and CK-MB in the cell supernatant were measured using commercial kits (Sino Best Biological Technology, China), following the respective instructions. The levels of tumor necrosis factor-α (TNF-α), interleukin 6 (IL-6), and IL-1β in cell supernatant were measured using commercial ELISA kits (Thermo Scientific-Pierce, China) following the guidelines stipulated by the manufacturer. The assays were conducted in triplicate.

CCK8 Assay

The Cell Counting Kit-8 (CCK8) from Psaitong, China, was utilized to assess cell viability. H9c2 cells (1×10^5 cells/mL) were cultured for 4 hours in 96-well plates and subsequently treated with APS-CS/TPP, HSP90AA1 inhibitor TAS-116. After 24-hour treatment, each well was administered 10 μL of CCK-8 solution and subsequently incubated at 37 °C for 2 hours. The optical density was measured at 450 nm using a 96-well plate reader (BIO-TEK Instruments, Inc).

The Wright Staining

H9c2 cells were cultured in 6-well plates, and one slide was placed in each well plate. H9c2 cardiomyocytes were treated with APS-CS/TPP for 6 hours. Subsequently, cells were treated with TAS-116 (0.2 mg/mL) for an additional 6 hours to observe more comprehensive morphological and pathological changes in cardiomyocytes. Wright staining was performed after washing with PBS. Finally, images were obtained under a microscope.

Western Blotting Analysis

The myocardial tissues and H9c2 cells were lysed in RIPA buffer (Servicebio, China) containing 1:100 PMSF (Servicebio, China). The concentration of all extracted proteins was quantified using the BCA protein analysis kit (Solarbio, China). Proteins were separated by SDS-PAGE using a 12% gradient gel and transferred onto 0.45 μm polyvinylidene fluoride (PVDF) membranes. After blocking with 5% skimmed milk, the following antibodies were used overnight at 4°C: rabbit anti-NLRP3 (1:1500, Gene Tex), rabbit anti-Hsp90AA1 (1:1000, Gene Tex), rabbit anti-Caspase -1 (1:1000, proteintech), rabbit anti-IL-1β (1:800, Gene Tex), and rabbit anti-beta-actin antibody (1:2000, Servicebio). The membranes were subsequently incubated with HRP-conjugated anti-rabbit IgGs (diluted 1:10000, provided by

Servicebio) at room temperature for 1 hour. The membranes were then processed using the enhanced chemiluminescence (ECL) detection system. ImageJ software was utilized for the quantification of the expression levels of the target proteins.

Statistical Analysis

All data were presented as the mean ± standard error of the mean (SEM) from at least three independent experiments and were analyzed using GraphPad Prism 9.0 software. Multiple group comparisons were conducted via one-way ANOVA using SPSS 22.0 software to assess statistical differences at $P < 0.05$. The survival curves was performed using the Kaplan-Meier method with the GraphPad Prism 5 software to assess statistical differences at $P < 0.05$.

Results

Predicting HSP90AA1 as a Key Target in APS Treating Septic Myocardial Injury

To predict the pharmacological mechanism of APS in treating septic myocardial injury, network pharmacology analysis was conducted. A total of 10 active ingredients of APS were collected from the HERB database and 264 compound-related targets were obtained through the Swiss Target Prediction database (Table 1). From the Genecards database, OMIM database, and Drugbank database, 2723 genes associated with septic myocardial injury were identified. Ultimately, 123 overlapping targets relevant to APS for the treatment of septic myocardial injury were selected using a Venn diagram (Figure 1A).

These potential genes were uploaded to the STRING database and used to construct a Protein-Protein Interaction (PPI) network to identify key targets, including HSP90AA1 (Figure 1B). To determine the critical pathways in which the hub targets were involved in APS against septic myocardial injury, KEGG signaling pathway analysis was conducted. The top-ranked pathways associated with the target protein HSP90AA1 were the NOD-like receptor signaling pathway (Figure 1C). Furthermore, to further clarify the interactions among hub targets, the active components of APS, HSP90AA1, and pathways, a drug-targets-pathway network was established using Cytoscape software. There were four components of APS that act on the core targets (fucose, galactose, glucose, rhamnose), which had higher degrees of interaction with HSP90AA1 and the NOD-like receptor signaling pathway (Figure 1D).

To further examine the interaction between APS and HSP90AA1, the analysis of molecular docking was conducted (Figure 2A). It was found that HSP90AA1 exhibited a higher binding affinity with fucose (−4.45 kcal/mol), galactose (−4.26 kcal/mol), glucose (−4.10 kcal/mol), and rhamnose (−3.97 kcal/mol), which are the main active compounds in APS. Therefore, HSP90AA1 is a specific target for APS, offering a novel strategy to reverse septic myocardial injury.

To further confirm the notion of molecular docking analysis indicating the tight intermolecular affinity between APS and HSP90AA1, an interaction between them was further examined by from MST assay. As expected, data revealed that APS had a high affinity to bind to HSP90AA1 with a Kd of 3.36±2.3nM (Figure 2B). Thus, HSP90AA1 is a specifically target for APS to provide a novel strategy to reverse septic myocardial injury.

Table 1 The Active Ingredients of APS

Ingredient_Id	Ingredient_Name	Ingredient_Smile
HBIN016562	Arabinose	C1C(C(C(C(O1)O)O)O)O
HBIN028037	Glucose	C(C1C(C(C(C(O1)O)O)O)O)O
HBIN024572	D-xylose	C1C(C(C(C(O1)O)O)O)O
HBIN048047	Vitamin c	C(C(C1C(=C(C(=O)O1)O)O)O)O
HBIN033605	L-rhamnose	CC1C(C(C(C(O1)O)O)O)O
HBIN023521	d-galacturonicacid	C1(C(C(OC(C1O)O)C(=O)O)O)O
HBIN024308	DL-Glucuronic acid	C(=O)C(C(C(C(C(=O)O)O)O)O)O
HBIN026805	Fucose	CC1C(C(C(C(O1)O)O)O)O
HBIN026990	Galactose	C(C1C(C(C(C(O1)O)O)O)O)O
HBIN018129	Beta-Glucan	C1C(C(OC(C1O)OC2C(C(OC(C2O)OC3C(COC(C3O)CO)O)CO)O)CO)O

https://doi.org/10.2147/IJN.S580840

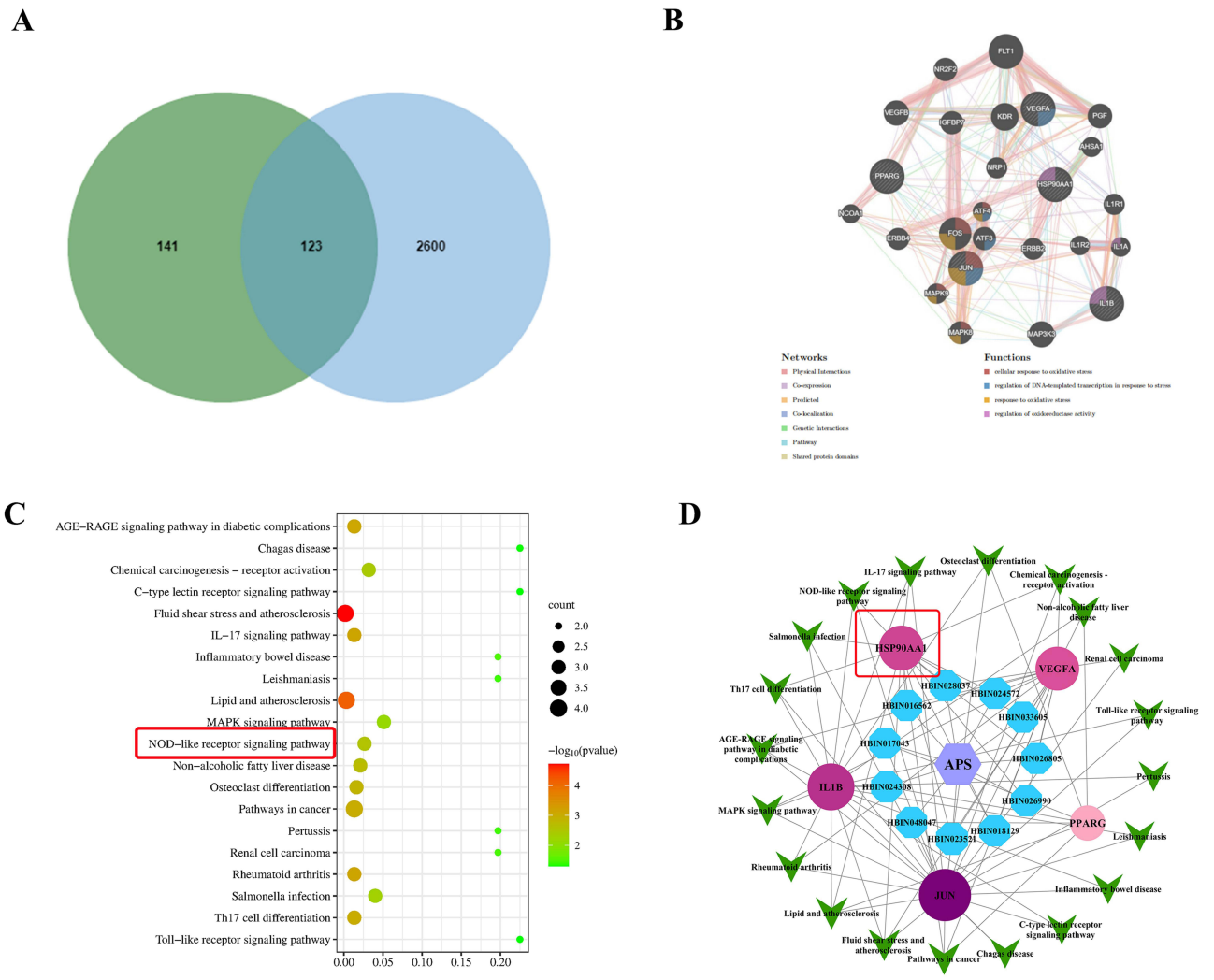

Figure 1 Network pharmacology predicted the potential therapeutic effects of APS on sepsis-induced myocardial injury via the NOD-like receptor signaling pathway. (**A**) To search for the overlapped targets of APS against septic myocardial injury, the Venny figure was utilized. (**B**) Core target proteins from the PPI network were identified using the MCODE algorithm. (**C**) KEGG enrichment analysis was performed using the DAVID database to explore signaling pathways. The red box highlights the strong association between sepsis-induced myocardial injury and the NOD-like receptor signaling pathway. (**D**) The drug-component-target-pathwaynetwork was visualized with the Cytoscape software. The red box indicates the higher interaction with the core components of APS and HSP90AA1.

Components of APS and Characterization of APS-CS/TPP

Analysis of monosaccharide composition of APS was necessary for structural characterization. It could be found that APS consisted of mannose (Man), rhamnose (Rha), glucose (Glc), galactose (Gal), fucose (Fuc), glucuronic acid (GlcA) and galacturonic acid (GalA). Additionally, the most hub portion of APS primarily contained Rha, Glc, Gal (Figure 3A).

To confirm the successful preparation of APS-CS/TPP, infrared spectroscopy was employed to detect the characteristic absorption peaks of both APS and the APS-CS/TPP. The results revealed a unique absorption peak at 618.3 cm^{-1} in the spectrum of the APS-CS/TPP, which was likely attributed to the connection site between APS and CS-TPP (Figure 3B). This finding confirmed the successful preparation of the APS-CS/TPP.

The characterization of APS-CS/TPP was investigated using the Zetasizer nano array to measure the size and ZETA (Figure 3C and D). The particle size of the APS-CS/TPP was relatively uniform, with an average of 186.35±0.31 nm. The ZETA potential results indicated that the APS-CS/TPP were positively charged with a value of +47.89±0.11 mV, demonstrating stable properties.

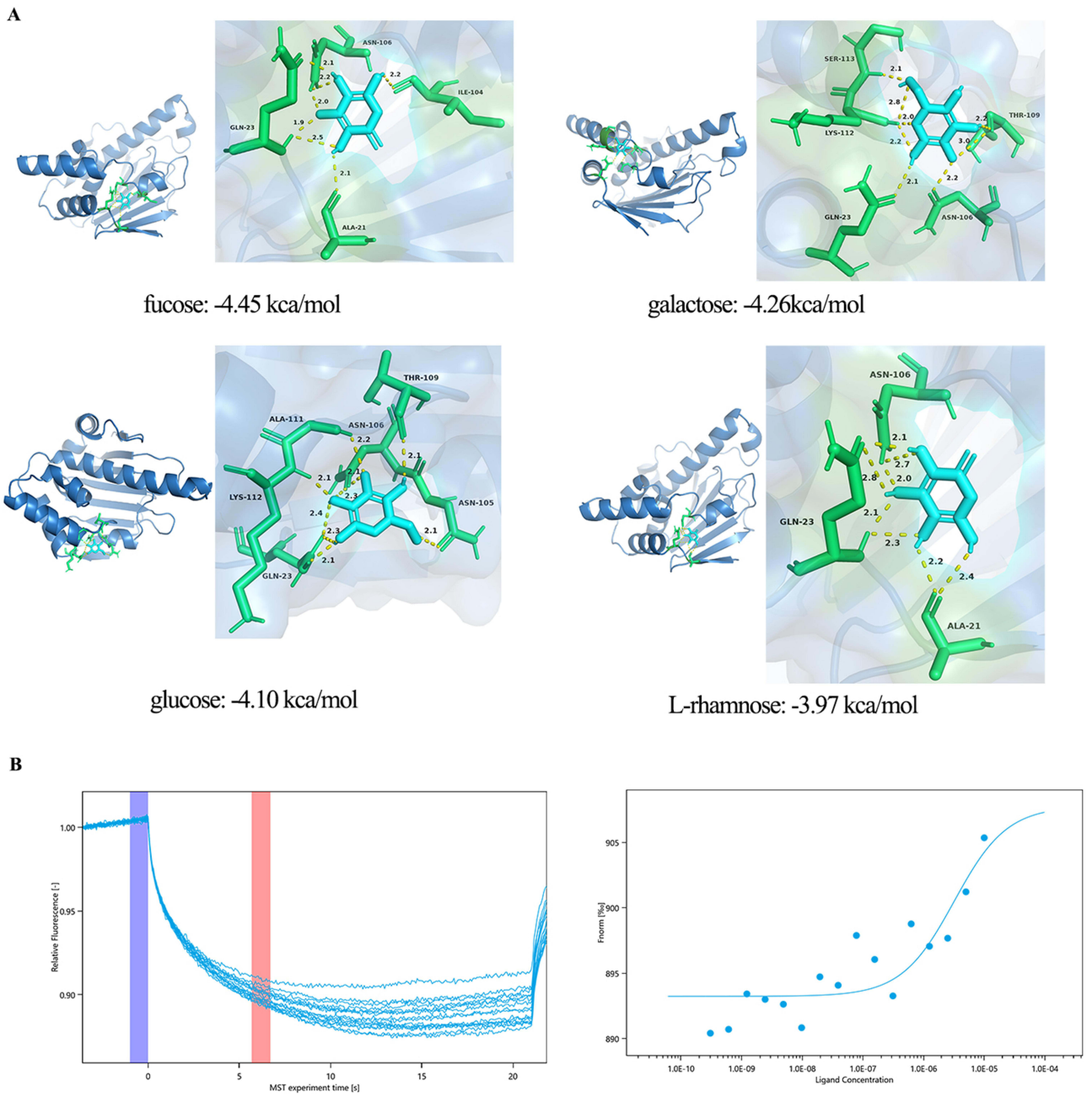

Figure 2 To further examine the interaction between APS and HSP90AAI using molecular docking and Microscale thermophoresis (MST). (**A**) Molecular docking was utilized to confirm the interaction between the HSP90AA1 and the core targets of APS polysaccharides. (**B**) The interaction between APS and HSP90AA1 was further verified APS had a high affinity to bind to HSP90AA1 by from MST assay.

APS-CS/TPP Alleviated Myocardial Injury in CLP-Induced Mice

To validate the protective effect of APS-CS/TPP on septic myocardial injury, an CLP-induced myocardial injury mice was applied (Figure 4A). As shown in Figure 4B, CLP led to a high mortality rate (66.67%). However, APS-CS/TPP overtly improved the survival rate compared to the CLP group (43.33%, $P<0.05$). Besides, echocardiography was used to evaluate the cardiac function of mice. Compared to the sham group, CLP resulted in severe myocardial injury, as evidenced by decreased LVEF, LVFS, SV as well as CO ($P<0.05$), while APS-CS/TPP treatment remarkably restored these CLP-induced pathological changes (Figure 4C and D). In addition, HE staining presented varying degrees of myocardial swelling, disordered myocardial fiber, expanded cell spaces, and inflammatory infiltration in the CLP model group. However, the pathological features of

https://doi.org/10.2147/IJN.S580840

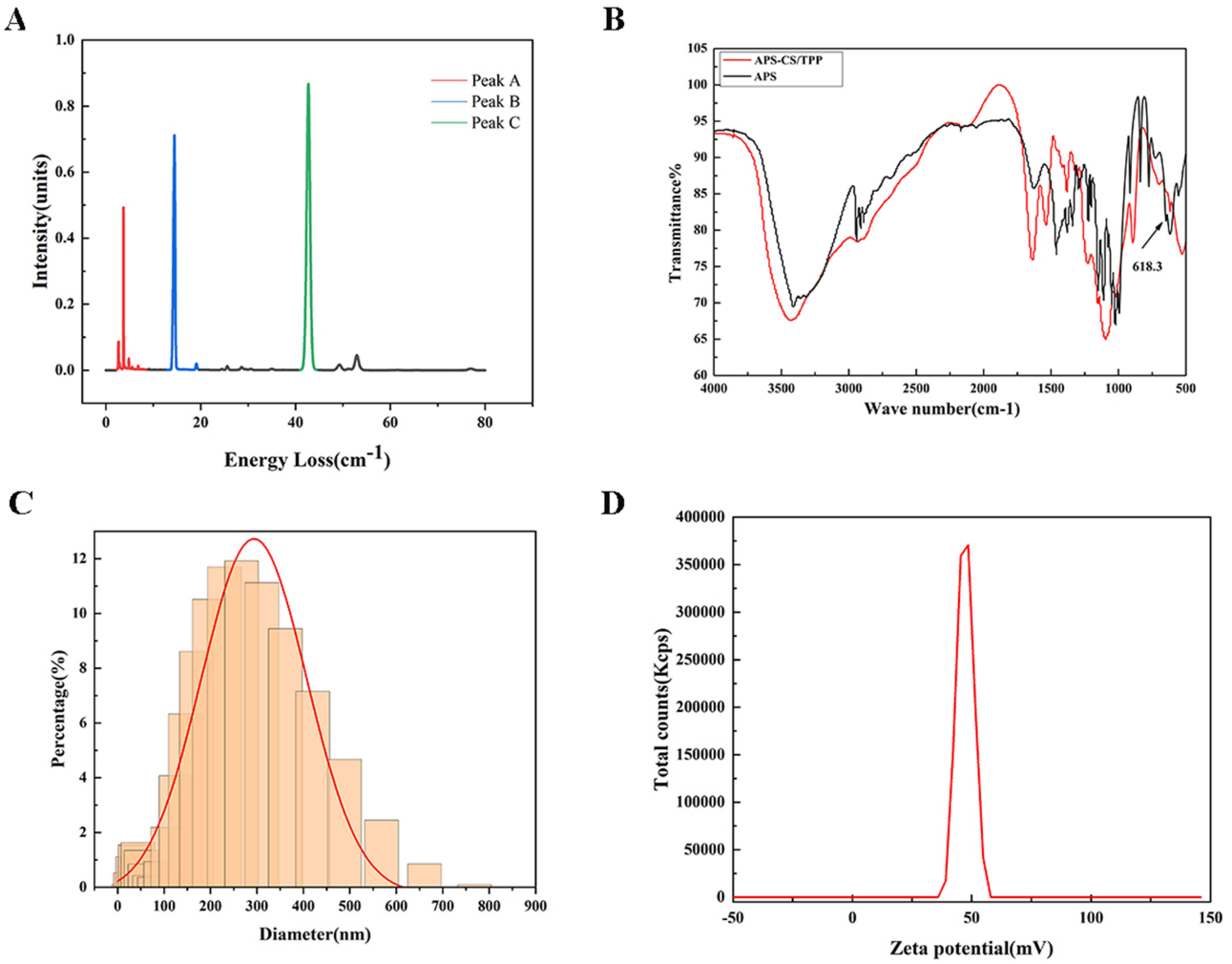

Figure 3 The components of APS and characterization of APS-CS/TPP. (**A**) The ingredients of APS was characterized via HPLC. The A, B, and C peaks correspond to rhamnose (Rha), glucose (Glc), galactose (Gal) respectively which correspond to the key components of APS. (**B**) The characteristic absorption peaks of APS and APS-CS /TPP using Infrared spectroscopy showed a unique absorption peak at 618.3 cm^{-1} in the spectrum of the APS-CS/TPP meaning the successful preparation of the APS-CS/TPP. (**C**) The size distribution of the APS-CS/TPP was relatively uniform, with an average of 186.35±0.31 nm. (**D**) The zeta potential values of APS-CS/TPP were positively charged with a value of +47.89±0.11 mV.

myocardial destruction were ameliorated in APS-CS/TPP group (Figure 4E). Moreover, APS-CS/TPP treatment reduced the serum levels of cTnI, CK-MB, and LDH (Figure 4F). Therefore, the results above suggested that APS-CS/TPP could alleviate septic myocardial injury in vivo.

APS-CS/TPP Regulating HSP90AA1 Impacts NLRP3 Signaling Pathway in vivo

To evaluate the impact of APS-CS/TPP on HSP90AA1 activity following CLP, we analyzed HSP90AA1 expression in the myocardial tissues using Western blotting. As shown in Figure 5A, APS-CS/TPP could downregulate the protein expression of the HSP90AA1/NLRP3 signaling pathway. Compared to the Sham group, the HSP90AA1 protein level was significantly increased in the CLP group but was reduced by APS-CS/TPP treatment (Figure 5B). Furthermore, to verify whether the suppression of HSP90AA1 activation by APS-CS/TPP was dependent on the NLRP3 pathway, the levels of NLRP3, caspase-1, and IL-1β were examined. The results revealed that APS-CS/TPP significantly decreased the levels of NLRP3, caspase-1, and IL-1β (P<0.01, Figure 5C–E), compared with those in the CLP groups.

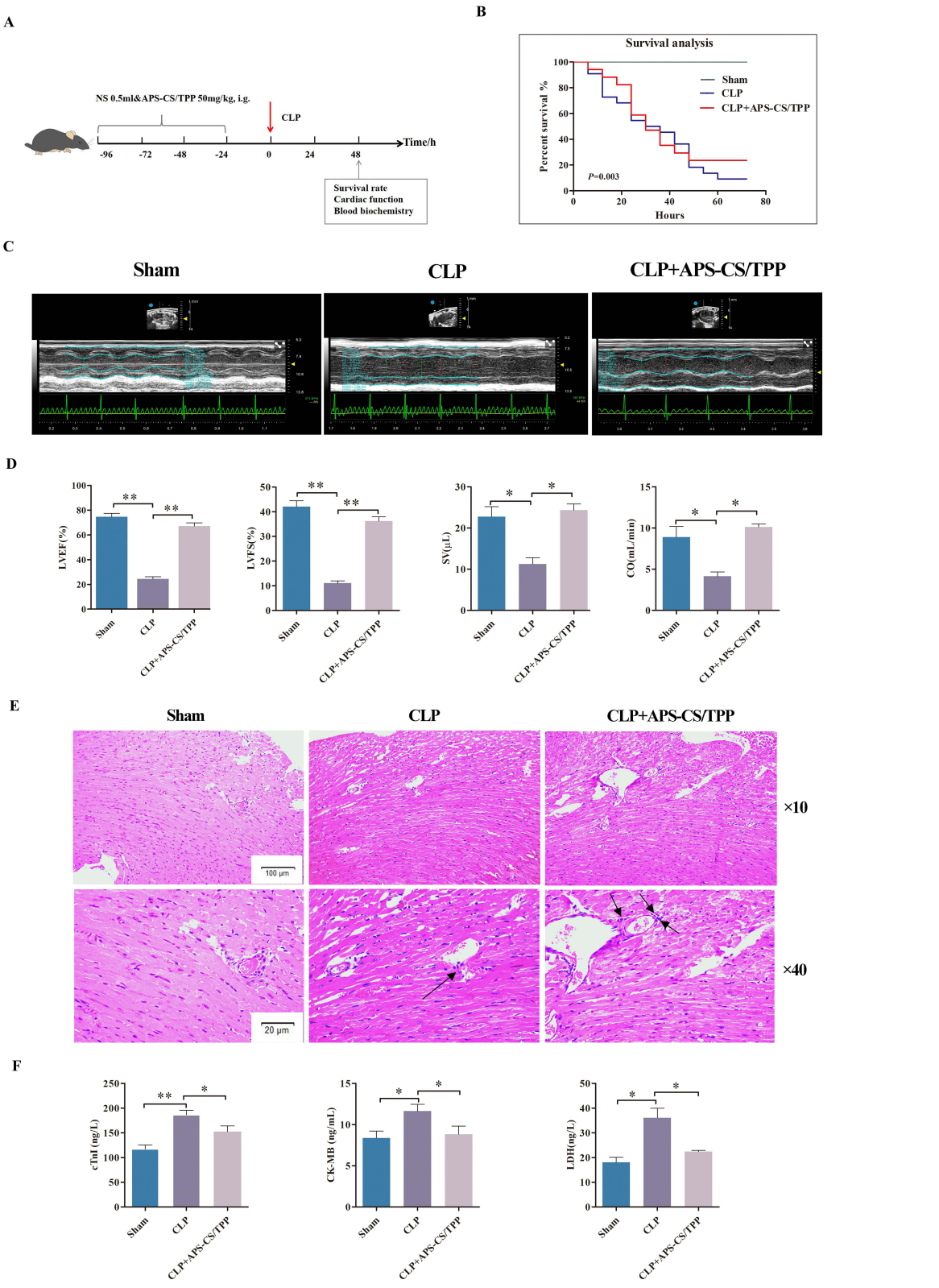

Figure 4 Effects of APS-CS/TPP on septic myocardial injury in vivo. (**A**) A schematic diagram of the experimental group and protocol. There were three groups: sham (n=22), model control group (CLP group, n=30), Astragalus polysaccharides nanoparticles group (CLP+APS -CS/TPP group, n=30) which were received gavage administration of 200mg/kg APS-CS/TPP once daily for 3 consecutive days prior to establish the CLP model. (**B**) The 72 h survival analysis of mice induced by CLP in each group. (**C**) Representative echocardiography images of the short axis using an animal specific transthoracic echocardiography at 8 h post-CLP in mice. (**D**) Statistical graph of LVEF, LVFS, SV as well as CO.*P<0.05,**P<0.01, compared with the CLP group. (**E**) Representative hematoxylin and eosin (H&E) stained sections of myocardial tissue from mice 48 h after cecal ligation and puncture (CLP) surgery. The black arrows indicate infiltrating inflammatory cells in the myocardial tissue. (**F**) Bar graphs of the levels of cTnI, CK-MB, and LDH in each group at 48 h post-CLP in mice.*P<0.05,**P<0.01, compared with the CLP group.

https://doi.org/10.2147/IJN.S580840

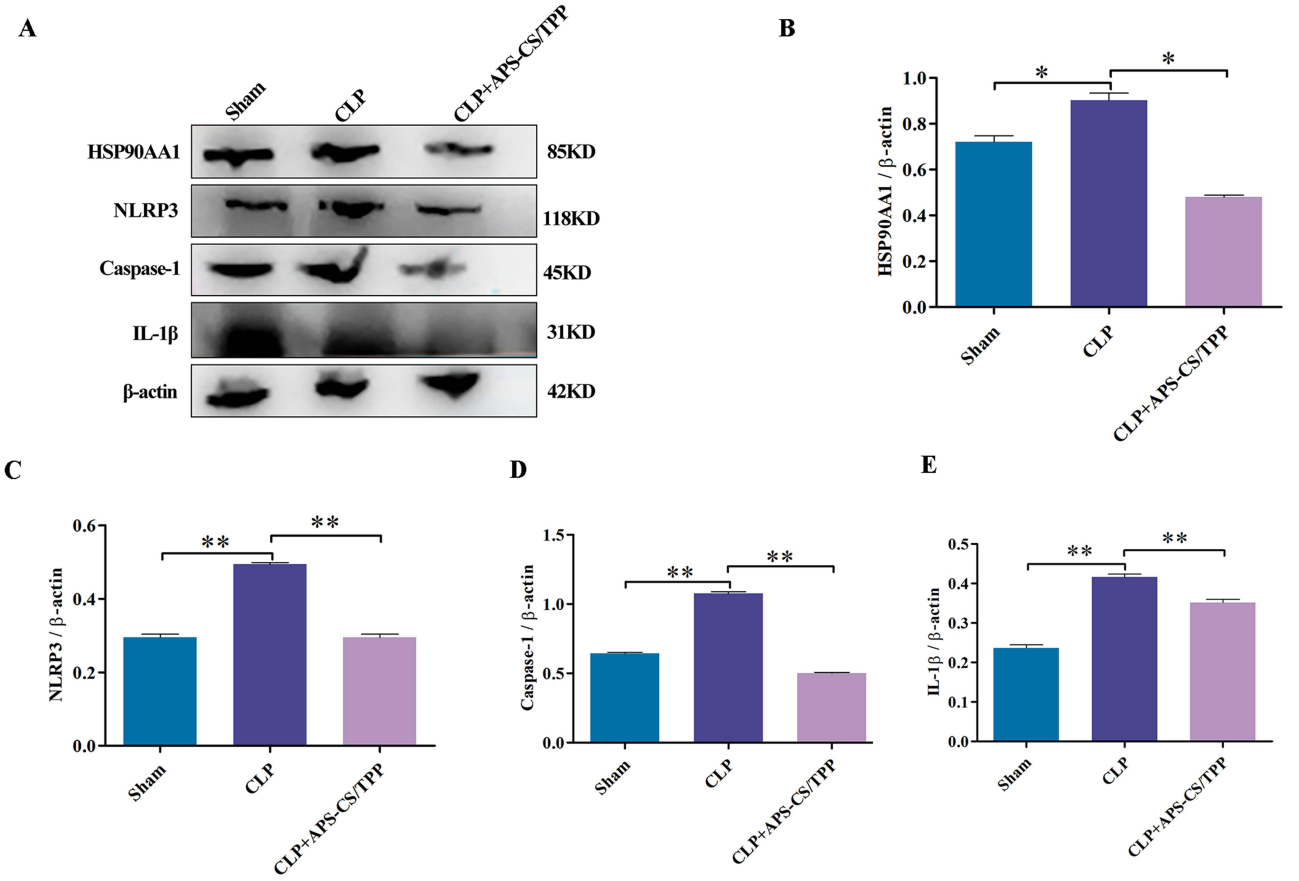

Figure 5 APS-CS/TPP inhibited the HSP90AA1/NLRP3 signaling pathway. (**A**) Representative images and (**B**–**E**) quantitative analysis of Western blots of HSP90AA1, NLRP3, Caspase-1, and IL-1B.*P<0.05,**P<0.01. Values are means± SD. The results represent three independent experiments.

APS-CS/TPP Alleviated the Cytotoxicity Induced by LPS in H9c2 Cells

Cell viability was assessed to investigate the function of APS-CS/TPP in LPS-induced myocardial cell damage using the CCK-8 assay. As showed in Figure 6A, after a 24 h incubation period, the cell viability of the LPS group was significantly reduced compared to the control group. However, upon treatment with APS-CS/TPP, the viability was notably higher ($P < 0.05$). However, after the inhibition of HSPAA1, the therapeutic efficacy of APS-CS/TPP significantly decreased. These results suggested that APS-CS/TPP could increase cell viability in LPS-induced H9c2 cells.

The cTNI and CK-MB levels as the cardiomyocyte injury-specific markers were analyzed in the cell culture supernatant by ELISA (Figure 6B and C). The results showed that compared to the LPS group, both levels of cTNI and CK-MB were significantly reduced by 23.3% and 28.3% in the LPS+APS-CS/TPP group (P<0.05), suggesting that APS-CS/TPP alleviated cardiac dysfunction in LPS-induced sepsis. However, upon administration of the HSP90AA1 inhibitor TAS-116, the therapeutic effect of APS-CS/TPP was affected. There was a statistically significant difference in cTnI and CK-MB levels between the LPS+APS-CS/TPP group and the LPS+TAS-116+APS-CS/TPP group.

The Wright staining results showed that the cellar integrity was damaged in the LPS group compared with the Control group resulting in irregular cell sizes. This damage was ameliorated by treatment with APS-CS/TPP. However, administration of TAS-116 still resulted in varying degrees of morphological damage (Figure 6D).

APS-CS/TPP Inhibited Inflammatory Cytokines in LPS-Induced H9c2 Cells

To investigate whether APS-CS/TPP attenuated septic myocardial injury by decreasing inflammatory cytokines secretion, the levels of key inflammatory markers (IL-1β, IL-6, and TNF-α) in cell supernatant were detected. As displayed in Figure 6E–G, the levels of IL-1β, IL-6, and TNF-α were remarkably increased in the LPS group compared with the Control group. APS-CS

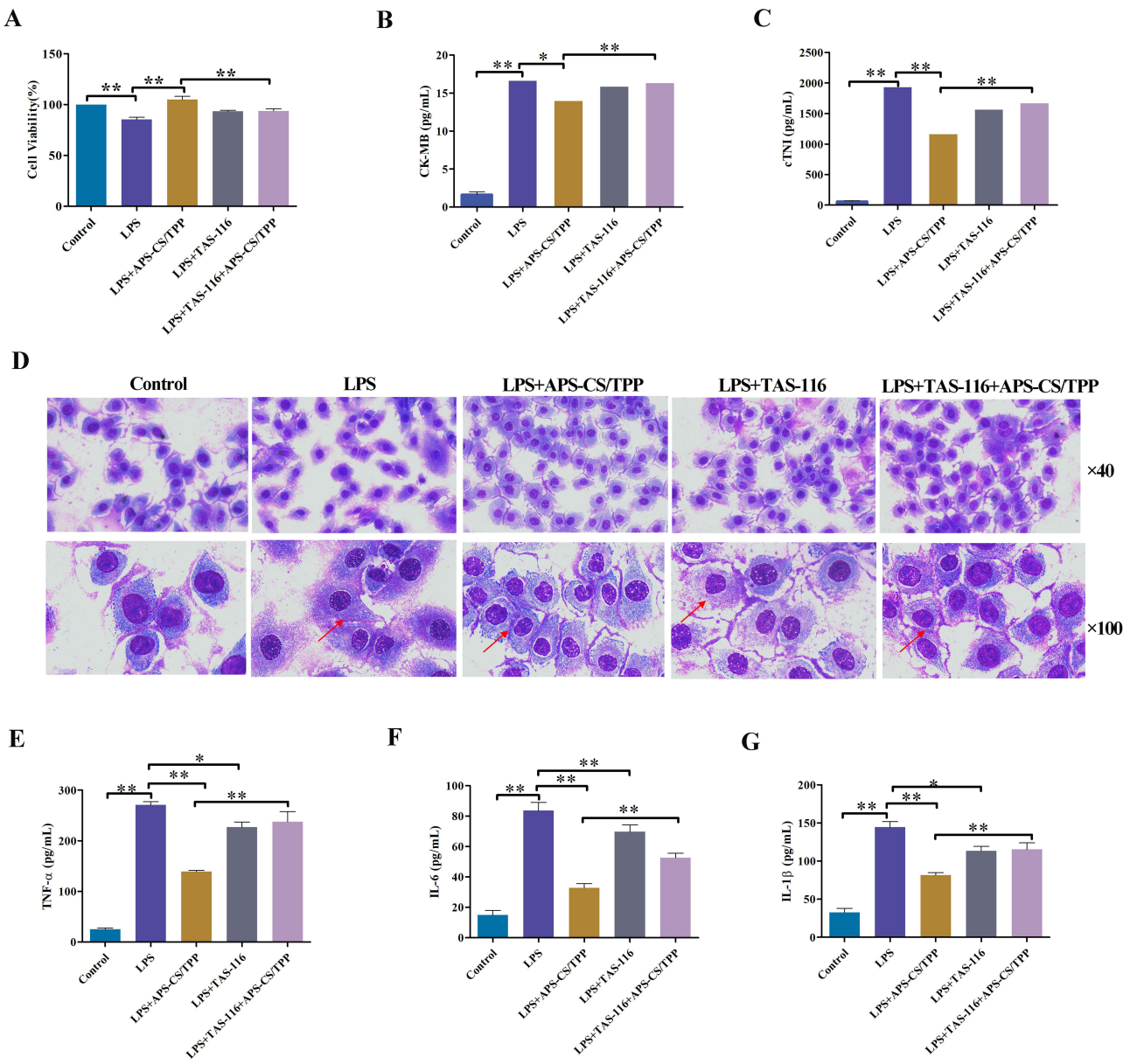

Figure 6 APS-CS/TPP suppressed inflammatory responses in LPS-induced H9c2 cells. (**A**) Cell viability was determined using the CCK-8 assay. (**B** and **C**) CK-MB and cTNI levels in LPS-induced H9c2 cells were measured by ELISA. (**D**) Morphological changes in H9c2 cardiomyocytes across groups were observed using Swiss staining. The red arrows indicate varying degrees of damage to the integrity of the cardiomyocyte cell membrane and cytoplasmic volume in each group. (**E**–**G**) The levels of TNF-α, IL-6, and IL-1β in LPS-induced H9c2 cells were determined by ELISA. The mean and standard deviation (n = 3 per group) represent the data. *$P < 0.05$, **$P < 0.01$, compared to the LPS group and the APS-CS/TPP group.

/TPP significantly inhibited the levels of IL-1β, IL-6, and TNF-α at least twice compared to the LPS group indicating that APS-CS/TPP had a strong anti-inflammatory effect. After treatment with the HSP90AA1 inhibitor TAS-116, however, there was a significant difference in inflammatory cytokine levels between the LPS+APS-CS/TPP group and the LPS+TAS-116 +APS-CS/TPP group, suggesting again that inhibition of the HSP90AA1 may influence the therapeutic effect of APS-CS/TPP.

Inhibition of the HSP90AA1 Activation by TAS-116 in LPS-Induced H9c2 Cells

To confirm the successful inhibition of the HSP90AA1 activation by TAS-116 in the experimental groups, Western blot analysis was performed to detect HSP90AA1 levels. After incubation with 0.2 mg/mL HSP90AA1 inhibitor TAS-116,

https://doi.org/10.2147/IJN.S580840

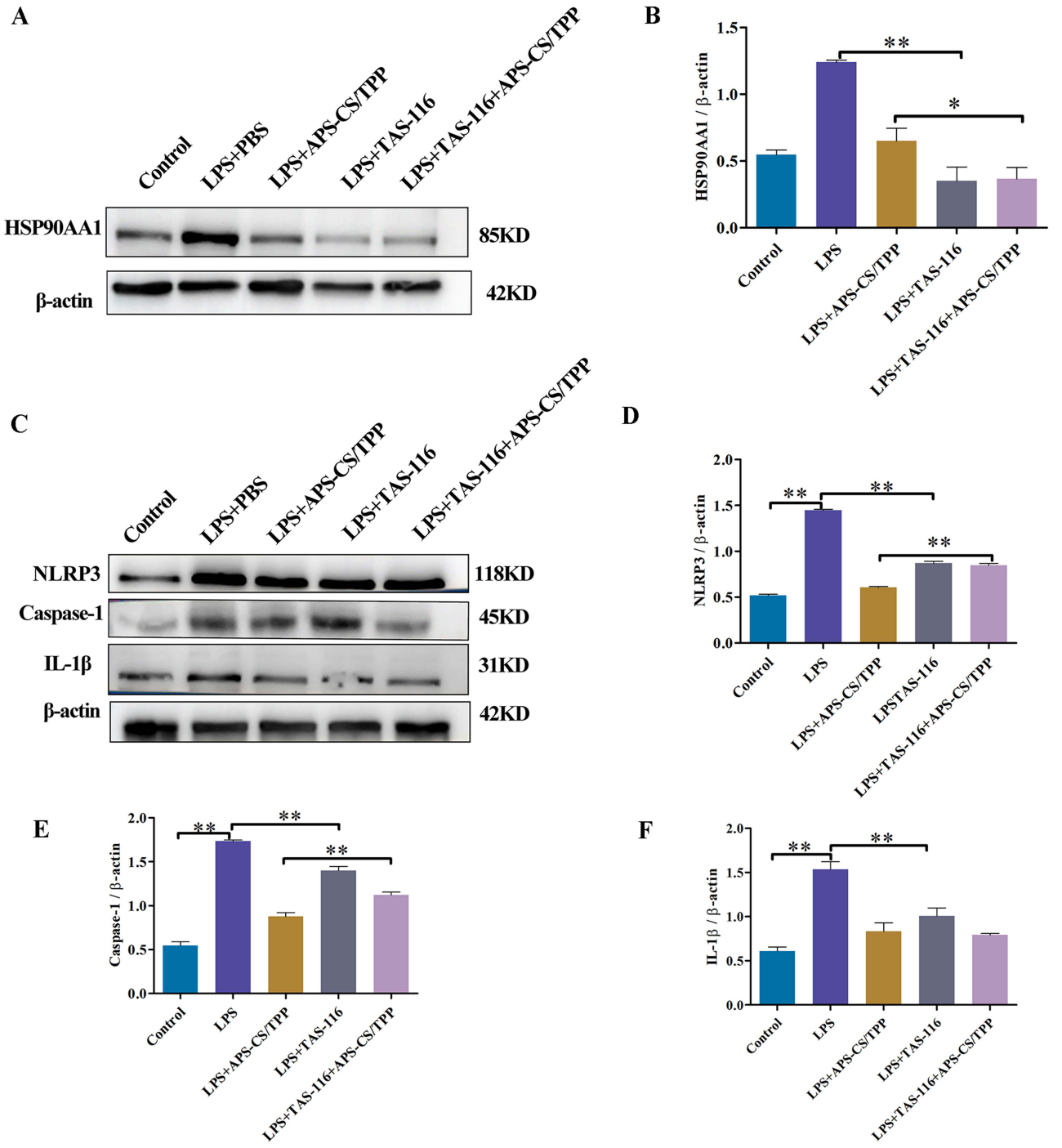

Figure 7 APS-CS/TPP attenuated protein expression in the HSP90AA1/NLRP3 signaling pathway in LPS-induced H9c2 cells. (**A** and **B**) Western blotting was used to visualize the successful inhibition of the HSP90AA1 activation by Tas-116 in the experimental groups. (**C**) Bands of NLRP3, Caspase-1, IL-1β, and β-actin were analyzed to verify whether the suppression of HSP90AA1 activation by APS-CS/TPP was dependent on the NLRP3 pathway. (**D**–**F**) The Western blot data was quantified using densitometric analysis and normalized to β-actin. **P*<0.05,***P*<0.01, compared to the LPS group and the APS-CS/TPP group.

HSP90AA1 levels in the LPS+TAS-116 and LPS+TAS-116+APS-CS/TPP groups were significantly lower compared to the LPS+PBS group, indicating successful inhibition of the HSP90AA1activation (Figure 7A and B).

APS-CS/TPP Inhibited the HSP90AA1/NLRP3 Signaling Pathway in LPS-Induced H9c2 Cells

To verify whether the suppression of HSP90AA1 activation by APS-CS/TPP was dependent on the NLRP3 pathway, the levels of NLRP3, Caspase-1, and IL-1β were analyzed. As shown in Figure 7C, the expression levels of NLRP3,

Caspase-1, and IL-1β revealed differences between the LPS+TAS-116+APS-CS/TPP group and the APS-CS/TPP group. The results revealed that APS-CS/TPP significantly decreased the levels of NLRP3, Caspase-1, and IL-1β ($P<0.01$, Figure 7D–F), compared with those in the LPS groups. These results demonstrated that APS-CS/TPP exerted a protective effect against septic myocardial injury potentially by modulating the NLRP3 pathway. HSP90AA1 had been identified as a novel target of APS-CS/TPP for the improvement of septic myocardial injury.

Discussion

For a long time, the treatment of septic myocardial injury has been a challenging issue worldwide. Apart from supportive treatment, there has been a notable absence of highly effective therapeutic drugs and methods.[17,18] In recent years, the utilization of nanomaterials for sepsis treatment has garnered significant interest due to their biocompatibility, precise targeting, and low toxicity.[19] For instance, gold nanoparticles (AuNPs) enhance the survival rate of septic mice by mitigating systemic inflammation.[20] Likewise, Casey et al developed cargo-less PLA/PLGA nanoparticles to study their anti-inflammatory effects on septic mice.[21] In this study, nanoparticles composed of APS and a chitosan nanocarrier were found to significantly enhance the survival rate and improve electrocardiogram readings. Furthermore, these APS-CS /TPP were capable of suppressing indicators of myocardial injury. This evidence has proven that APS-CS/TPP therapy was beneficial for septic myocardial injury. Nonetheless, it remained challenging to fully elucidate the mechanisms by which APS-CS/TPP treat septic myocardial injury. Consequently, we employed a network pharmacology approach to systematically investigate the mechanisms of APS-CS/TPP in protecting against septic myocardial injury.

Upon analyzing the constructed herb-compound-target network, it was determined that fucose, galactose, glucose, and rhamnose are the active ingredients associated with the majority of the targets. Additionally, the analysis of monosaccharide composition of APS via HPLC also showed a portion of APS may contain galactose, glucose, and rhamnose. Consequently, the multiple active compounds in APS could effectively treat septic myocardial injury. Upon analyzing the target interaction network, JUN, IL1β, VEGFA, and HSP90AA1 were identified as central to the entire network, which can be considered the key targets of APS in treating septic myocardial injury. The molecular docking and MST results indicated that HSP90AA1 exhibits good binding properties with the main active components of APS. Previous studies have suggested that HSP90AA1 acted on specific targets of APS in the treatment of pulmonary fibrosis.[22.]

Hsp90AA1, one of the most abundant and conserved chaperones, was a potential therapeutic target for heart disease.[23,24] These were the hub genes of heart failure (HF), playing a critical role in the oxidative stress associated with HF.[25] It has also been indicated that it plays a vital role in the process of myocardial ischemia/reperfusion (I/R) injury and is a novel target of miR-1 during myocardial I/R.[26] Several studies have investigated HSP90AA1 in sepsis. Wang et al have demonstrated that HSP90AA1 significantly decreased the LPS-induced elevation of ROS production and reduced nitric oxide release in RAW264.7 cells.[27] In CLP rats, HSP90AA1 was increased in pathogenesis of Atrial fibrillation regulating lipid biosynthesis.[28] In our study, the protein level of HSP90AA1 was also elevated in LPS-induced H9c2 cells. However, following treatment with APS-CS/TPP, the viability was significantly restored, the Cellular morphology was ameliorated, and the levels of circulating myocardial markers, cTNI and CK-MB, were reduced in H9c2 cells.

APS possess excellent anti-inflammatory properties, not only suppressed NF-κB activation but also inhibited MAPK pathways in LPSstimulated RAW264.7.[29] In this study, the KEGG enrichment analysis indicated that the pharmacological mechanisms of APS in septic myocardial injury might be primarily associated with the NOD-like receptor signaling pathway. Further in vivo and vitro study revealed that APS-CS/TPP could attenuate sepsis myocardial injury by decreasing proinflammatory cytokines secretion through the inhibition of HSP90AA1/NLRP3 signaling pathway. HSP90AA1 proteins were major stabilizing factors for NLR proteins. More recent studies indicated that HSP90 facilitated NLRP3 inflammasome activity during infections and inflammatory diseases.[30,31] Choudhury et al demonstrated that HSP90 played a significant role in the regulation of NLRP3 inflammasome activity and downstream IL-1β and IL-18 secretion in alcoholic liver injury.[32] Inhibition of HSP90 significantly decreased the secretion of IL-1β and IL-18. This demonstrated that HSP90 could promote proinflammatory cytokines, and its inhibition in vivo could attenuate LPS-mediated inflammation.[33] Consistently, Our data identified treatment with an HSP90AA1 inhibitor TAS-116, which suppresses HSP90AA1 activity, similarly abolished the therapeutic effect of APS-CS/TPP. APS-CS/TPP could reduce IL-1β, IL-6 and TNF-α secretion in the HSP90AA1/NLRP3 axis during therapeutic treatment in septic myocardial injury. Notably, this made the first instance of revealing the potential

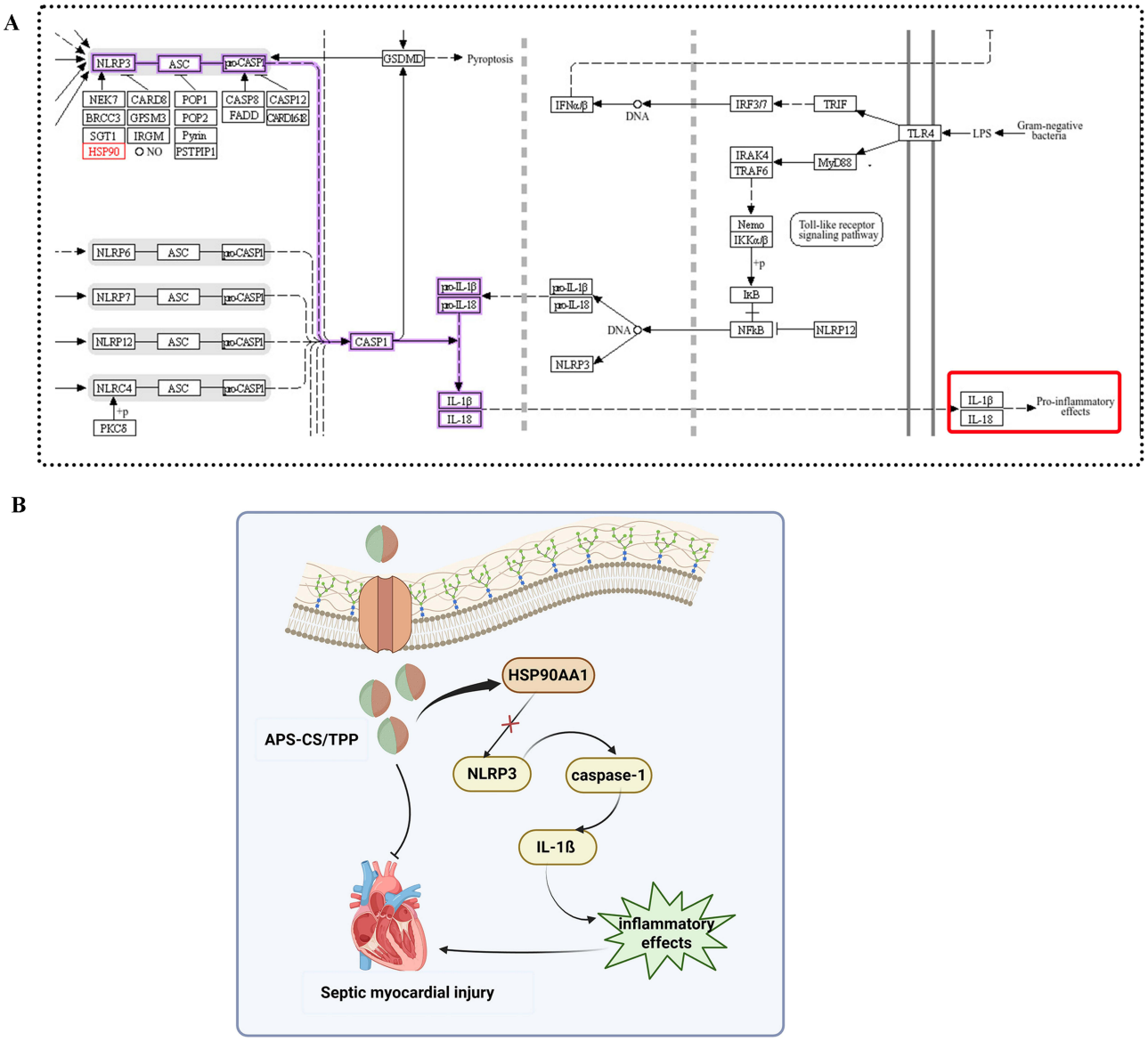

Figure 8 APS-CS/TPP intervene in septic myocardial injury, involving the HSP90AA1/NLRP3 signaling pathway. (**A**) Schematic diagram of the HSP90AA1/NLRP3 signaling pathway. The purple box designates the Hsp90AA1/NLRP3 signaling pathway, and the red box indicates the inflammatory effects ultimately produced by this pathway. (**B**) APS-CS/TPP suppressed the release of inflammatory cytokines while reducing the protein levels of HSP90AA1, NLRP3, caspase-1, and IL-1β.

targets and mechanisms of APS-CS/TPP in treating septic myocardial injury by inhibiting the HSP90AA1/NLRP3 signaling pathway.

In conclusion, this study demonstrated that APS-CS/TPP exhibited significant protective activity against septic myocardial injury in both CLP mice and LPS induced H9c2 cells. Additionally, APS-CS/TPP exerted protective effect in septic myocardial injury by modulating the HSP90AA1/NLRP3 signaling pathway. This discovery offered valuable insights into the protective mechanism of APS-CS/TPP, suggesting that it may have therapeutic potential for septic myocardial injury. However, further studies are needed to explore the clinical applicability of APS-CS/TPP in septic myocardial injury treatment.

Conclusion

This study elucidated the mechanisms by which APS-CS/TPP intervene in septic myocardial injury, involving the HSP90AA1/NLRP3 signaling pathway (Figure 8). Furthermore, this discovery offered valuable insights, identifying

HSP90AA1 as a novel intervention target for APS to reverse septic myocardial injury. While this preclinical study identifies a novel mechanistic insight, its translational relevance to HSP90AA1/NLRP3 and septic myocardial injury requires further investigation. Future research should aim to validate this target in clinical contexts, which could pave the way for new therapeutic strategies. A key limitation is the focus on acute-phase injury, which limits insights into long-term cardiac function. The mechanistic findings, derived from model systems, necessitate future validation in clinical settings.

Abbreviations

APS-CS/TPP, Astragalus polysaccharide nanoparticles; APS, Astragalus polysaccharide; cTnT, Cardiac troponin T; CK-MB, Creatine Kinase-MB; ECL, Enhanced chemiluminescence; Hsp90AA1, Heat Shock Protein 90 Alpha Family Class A Member 1; MST, Microscale thermophoresis; NLRP3, NOD like receptor protein 3; PVDF, polyvinylidene fluoride; IL-6, interleukin 6; SEM, standard errors of the means; TNF-α, tumornecrosis factor-α.

Data Sharing Statement

The data that support the findings of this study are available from the corresponding author upon reasonable request.

Ethics Approval

All animal experiments were approved by the Experimental Animal Center of Lanzhou University. Animal experiments were carried out in compliance with the Guide for the Animals Care and Ethics Committee of the first Hospital of Lanzhou University (Approval No. LDYYLL2023-127). The study conformed to the Guide for the American Veterinary Medical Association (AVMA Guidelines for the Euthanasia of Animals: 2020 Edition).

Funding

This work was supported by the National Natural Science Foundation of China (82360800), the Natural Science Foundation of Gansu Province (21JR1RA087), and a grant from the Health Commission of Gansu Province (GSWSQN2024-05).

Disclosure

The authors declare that they have no known competing financial interests or personal relationships that could have appeared to influence the work reported in this paper.

References

1. Erdem A, Meltem Sevgili A, Akbiyik F, et al. Tezosentan attenuates organ injury and. mesenteric blood flow decrease in endotoxemia and cecal ligation and puncture. *J Surg Res*. 2007;141:211–219. doi:10.1016/j.jss.2006.08.028
2. Sharma AC, Motew SJ, Farias S, et al. Sepsis alters myocardial and plasma concentrations. of endothelin and nitric oxide in rats. *J Mol Cell Cardiol*. 1997;29:1469–1477. doi:10.1006/jmcc.1997.0386
3. Rumery K, Yunus F, Frishman WH. Myocardial Depression in sepsis: beneficial adaptation. or sequelae that requires treatment? *Cardiol Rev*. 2020;28:256–261. doi:10.1097/CRD.0000000000000301
4. Hotchkiss RS, Moldawer LL, Opal SM, et al. Sepsis and septic shock. *Nat Rev Dis Primers*. 2016;2(1):16045. doi:10.1038/nrdp.2016.45
5. Wu Y, Zhang Y, Zhang J, et al. Cathelicidin aggravates myocardial ischemia/reperfusion injury via activating TLR4 signaling and P2X7R/NLRP3 inflammasome. *J Mol Cell Cardiol*. 2020;139:75–86. doi:10.1016/j.yjmcc.2019.12.011
6. Jo EK, Kim JK, Shin DM, et al. Molecular mechanisms regulating NLRP3 inflammasome activation. *Cell Mol Immunol*. 2016;13(2):148–159. doi:10.1038/cmi.2015.95
7. He W, Dong H, Wu C, et al. The role of NLRP3 inflammasome in sepsis: a potentialtherapeutic. target. *Int Immunopharmacol*. 2023;115:109697. doi:10.1016/j.intimp.2023.109697
8. Giguère PM, Gall BJ, Ezekwe EA, et al. G Protein signaling modulator-3 inhibits the inflammasome activity of NLRP3. *J Biol Chem*. 2014;289 (48):33245–33257. doi:10.1074/jbc.M114.578393
9. Zheng W, Su H, Lv X, et al. Exon-INTRON circular RNA circRNF217 Promotes innate immunity. and antibacterial activity in teleost fish by reducing miR-130-3p function. *J Iimmunol*. 2022;208(5):1099–1114. doi:10.4049/jimmunol.2100890
10. Wan Y, Xu L, Wang Y, et al. Preventive effects of astragaloside IV and its active sapogenin cycloastragenol on cardiac fibrosis of mice by inhibiting the NLRP3 inflammasome. *Eur J Pharmacol*. 2018;833:545–554. doi:10.1016/j.ejphar.2018.06.016

11. Shaaban AA, Abdelhamid AM, Shaker ME, et al. Combining the HSP90 inhibitor Tas-116 with metformin effectively degrades the NLRP3 and attenuates inflammasome activation in rats: a new management paradigm for ulcerative colitis. *Biomed Pharmacothe*. 2022;153:113247. doi:10.1016/j.biopha.2022.113247
12. Yang CX, Chen L, Mou Q, et al. HSP90AA1 promotes viability and lactate production but inhibits hormone secretion of porcine immature Sertoli cells. *Theriogenology*. 2022;194:64–74. doi:10.1016/j.theriogenology.2022.09.027
13. Abuelsaad ASA; Abuelsaad AS. Supplementation with Astragalus polysaccharides alters Aeromonas-induced tissue-specific cellular immune response. *Microb Pathogenesis*. 2014;66:48–56. doi:10.1016/j.micpath.2013.12.005
14. Li W, Shao C, Huang P, et al. Optimization, characterization of Astragalus polysaccharides, and evaluation of anti-inflammation effect in primary cultured astrocytes via HMGB1/RAGE/NF-κB/NLRP3 signal pathway. *Ind Crops Prod*. 2023;197:116594. doi:10.1016/j.indcrop.2023.116594
15. Minghua L, Jingnan W, Jiayun T. Preparation, complexation mechanism and properties of nano-complexes of Astragalus polysaccharide and amphiphilicchitosan derivatives. *Carbohydr Polym*. 2017;161:261–269. doi:10.1016/j.carbpol.2016.12.068
16. Xu X, Rui S, Chen C, et al. Protective effects of astragalus polysaccharide nanoparticles on septic cardiac dysfunction through inhibition of TLR4/NF-κB signaling pathway. *Int J Biol Macromol*. 2020;153:977–985. doi:10.1016/j.ijbiomac.2019.10.227
17. Xu S, Zhou Q, Jiang Z, et al. The effect of doxycycline-containing chitosan/carboxymethyl chitosan nanoparticles on NLRP3 inflammasome in periodontal disease. *Carbohydr Polym*. 2020;237:116163. doi:10.1016/j.carbpol.2020.116163
18. Gotts JE, Matthay MA. Sepsis: pathophysiology and clinical management. *BMJ*. 2016;353:i1585. doi:10.1136/bmj.i1585
19. Chen L, Huang Q, Zhao T, et al. Nanotherapies for sepsis by regulating inflammatory signals and reactive oxygen and nitrogen species: new insight for treating COVID-19. *Redox Biol*. 2021;45:102046. doi:10.1016/j.redox.2021.102046
20. Taratummarat S, Sangphech N, Ctb V, et al. Gold nanoparticles attenuates bacterial sepsis in cecal ligation and puncture mouse model through the induction of M2 macrophage polarization. *BMC Microbiol*. 2018;18:85. doi:10.1186/s12866-018-1227-3
21. Casey LM, Kakade S, Decker JT, et al. Cargo-less nanoparticles program innate immune cell responses to toll-like receptor activation. *Biomaterials*. 2019;218:119333. doi:10.1016/j.biomaterials.2019.119333
22. Bing P, Zhou W, Tan S. Study on the mechanism of astragalus polysaccharide in treating pulmonary fibrosis based on "drug-target-pathway" network. *Front Pharmacol*. 2022;13:865065. doi:10.3389/fphar.2022.865065
23. Ganekal P, Vastrad B, Vastrad C, et al. Identification of biomarkers, pathways, and potential therapeutic targets for heart failure using next-generation sequencing data and bioinformatics analysis. *Therapeut Adv Cardiovasc Dis*. 2023;17:17539447231168471. doi:10.1177/17539447231168471
24. Liu L, Zhang Y, Du Y, et al. The therapeutic effect and targets of cellulose polysaccharide on coronary heart disease (CHD) and the construction of a prognostic signature based on network pharmacology. *Frontiers in Nutrition*. 2022;9:986639. doi:10.3389/fnut.2022.986639
25. Gu J, Zhang LN, Gu X, et al. Identification of hub genes associated with oxidative stress in heart failure and their correlation with immune infiltration using bioinformatics analysis. *PeerJ*. 2023;11:e15893. doi:10.7717/peerj.15893
26. Zhu WS, Guo W, Zhu JN, et al. Hsp90aa1: a novel target gene of miR-1 in cardiac ischemia/reperfusion injury. *Sci Rep*. 2016;20166:24498. doi:10.1038/srep24498
27. Wang Y, Xiong Z, Li C, et al. Multiple beneficial effects of aloesone from *Aloe vera* on LPS-Induced RAW264.7 cells, including the inhibition of oxidative stress, inflammation, M1 polarization, and apoptosis. *Molecules*. 2023;28:1617. doi:10.3390/molecules28041617
28. Fang Y, Wu Y, Liu L, et al. The four key genes participated in and maintained atrial fibrillation process via reprogramming lipid metabolism in AF patients. *Front Genetics*. 2022;13:821754. doi:10.3389/fgene.2022.821754
29. Guangming C, Nan J, Junping Z, et al. Structural characterization and anti-inflammatory activity of polysaccharides from Astragalus membranaceus. *Int J Biol Macromol*. 2023;241:124386. doi:10.1016/j.ijbiomac.2023.124386
30. Mayor A, Martinon F, De Smedt T, et al. A crucial function of SGT1 and HSP90 in inflammasome activity links mammalian and plant innate immune responses. *Nat Immunol*. 2007;8(5):497–503. doi:10.1038/ni1459
31. Kadota Y, Shirasu K, Guerois R. NLR sensors meet at the SGT1-HSP90 crossroad. *Trends Biochem Sci*. 2010;35:199–207. doi:10.1016/j.tibs.2009.12.005
32. Choudhury A, Bullock D, Lim A, et al. Inhibition of HSP90 and activation of HSF1 diminish macrophage NLRP3 inflammasome activity in alcohol-associated liver injury. *Alcohol Clin Exp Res*. 2020;44:1300–1311. doi:10.1111/acer.14338
33. Ambade A, Catalano D, Lim A, et al. Inhibition of heat shock protein 90 alleviates steatosis and macrophage activation in murine alcoholic liver injury. *J Hepatol*. 2014;61(4):903–911. doi:10.1016/j.jhep.2014.05.024